Supporting information for: Simple peptide coacervates adapted for rapid pressure-sensitive wet adhesion

Ilia Kaminker,[1,a] Wei Wei,[2,1] Alex M. Schrader,[3] Yeshayahu Talmon,[4] Megan T. Valentine,[2,5] Jacob N. Israelachvili,[2,3,6] J. Herbert Waite,[2,6,7] Songi Han[1,3]

1. Department of Chemistry and Biochemistry, University of California Santa Barbara, CA 93106 USA
2. Materials Research Laboratory, University of California Santa Barbara, CA 93106 USA
3. Department of Chemical Engineering, University of California Santa Barbara, CA 93106 USA
4. Department of Chemical Engineering and the Russell Berrie Nanotechnology Institute (RBNI), Technion-Israel Institute of Technology, Haifa 3200003, Israel.
5. Department of Mechanical Engineering, University of California Santa Barbara, CA 93106 USA
6. Biomolecular Science and Engineering Program, University of California Santa Barbara, CA 93106 USA
7. Department of Molecular, Cell and Development Biology, University of California, Santa Barbara CA 93106 USA

Mfp3 peptide sample preparation

Custom synthesized peptide sequences of mfp-3S-pep, mfp-3F-pep and their variants (Table S1) were purchased from GenScript. The peptide powder was dissolved in 5% Acetic Acid / 8M Urea aqueous solution and injected into the Aquapore column of a reversed phase high performance liquid chromatography system (HPLC, 260 × 7 mm RP-300 Applied Biosciences Inc., Foster City, CA), and eluted with a 30 minutes long linear gradient of aqueous acetonitrile. The most concentrated fractions, as judged by optical absorption at 280nm were combined and freeze-dried. After freeze drying the mfp3s-pep samples were dissolved in 100mM acetic acid aqueous solution and the mfp3f-pep samples were dissolved in 10mM sodium acetate (pH5.5) solution. Peptide concentration was determined by optical absorption at 280nm, and samples were stored at -20°C before use. Concentrations were determined using extinction coefficients which were calculated using the ProtParam server: $\xi_{mfp\text{-}3S\text{-}pep}$ = 26930 and $\xi_{mfp\text{-}3F\text{-}pep}$ = 14440 for mfp-3S-pep and mfp-3F-pep respectively.

Spin labeled peptides were prepared by dissolving ~1mg of the peptide powder in 1ml 5% acetic acid 8M Urea aqueous solution, adding 10µl of 340mM MTSL spin label in DMSO stock and incubating the reaction overnight. The spin labelled peptides were subjected to HPLC purification as described in the previous paragraph. Since spin labeling increases the elution time of the peptides only the fractions corresponding to the peak with the longest elution time were retained in this case. In this approach it was possible to resolve spin labelled and unlabeled peptides during the HPLC purification, ensuring essentially 100% spin labelling efficiency for our samples.

Mfp-3S-pep (including mfp-3S-pepSL) coacervates were prepared by adding aqueous 5M NaCl solution to a final concentration of 0.6M NaCl and thoroughly mixing. Mfp-3F-pep / HA (including mfp-3F-pepSL and HA-SL) were prepared by thorough mixing of the mfp-3F-pep peptide and HA (typically 2-6 mg/ml) solutions to arrive at the final sample with equal weight - amounts of mfp-3F-pep and HA. Fresh samples were prepared before each measurement and formation of coacervate in every case was visually confirmed by observing the increase in the turbidity. In cases when a mixture of spin-labelled and non-

[1] These authors contributed equally to this work

spin-labelled peptides was used, the two peptide solutions were mixed first followed by addition of NaCl or HA for mfp-3S-pep and mfp-3F-pep coacervate formation respectively.

Table S 1 Peptide sequences used in this study. (Underline highlights the cysteine residues used for spin labelling)

mfp-3F-pep	GNYKYRGYGYPRGWKKGRKYY
mfp-3F-pepSL	GNYKYRGYGYPCRGWKKGRKYY
mfp-3S-pep	GYDGYNWPYGYNGYRYGWNKGWNGY
mfp-3S-pepSL	GYDGYNWPYGYNCGYRYGWNKGWNGY
mfp-3S-pepSL2	CGYDGYNWPYGYNGYRYGWNKGWNGY

Confocal microscopy

Three dimensional confocal images were recorded using Olympus Fluoview 1000 Spectral Confocal inverted microscope with 60x silicon oil immersion objective. For coacervate imaging the peptides were incubated with Acridine orange dye for 15 minutes before the beginning of the experiment. The excitation and emission wavelengths were 488nm and 526nm respectively. The in-plane pixel size was 0.207µm and the xy plane was acquired every ~0.2µm.

Confocal microscopy on hydrophobic surface

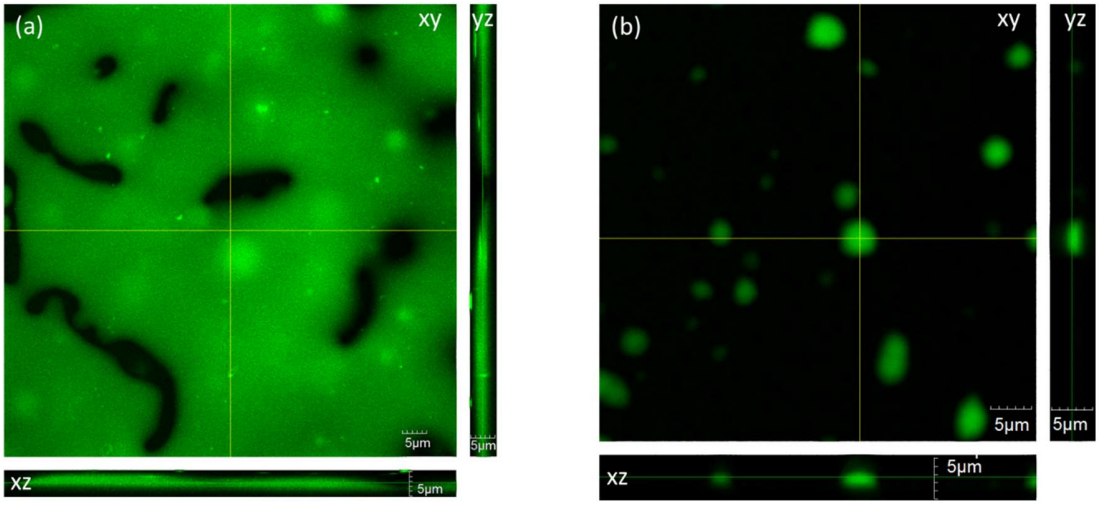

Figure S1. Confocal micrographs of (a) mfp-3F-pep / HA complex coacervate and (b) mfp-3S-pep single component coacervate deposited on an alkylated glass surface. The samples shown were allowed to settle for ~30min prior to imaging. Yellow lines denote the positions of the cross sections in other views.

Microrheology.

Microrheology measurements were performed on the two coacervate phases by analyzing the trajectories of 40-nm fluorescent nanoparticles embedded in the liquid (FluoSpheres®, 0.04 µm, red-orange fluorescent (565/580), ThermoFisher Scientific) and imaged as a sequence of confocal

micrographs. The nanoparticles were admixed to the peptides prior to coacervate formation and encapsulated inside the coacervate phase upon coacervate formation. After deposition on the glass, coacervates were allowed to settle for ~30min to ensure no new coacervate droplets would be sedimented inside of the field of view and confocal micrographs were acquired. The focal plane was chosen to be few μm above the glass surface inside the coacervate layer deposited on the glass surface.

For particle tracking, confocal images were recorded using Olympus Fluoview 1000 Spectral Confocal inverted microscope with 60x silicon oil immersion objective. Images were acquired every 3.28s; the in-plane magnification was 34nm/pixel. The wavelengths were 559nm and 603nm for excitation and emission respectively. Several sequences focusing on different parts of the sample were recorded and subsequently analyzed for particle motion. Examples of such image sequences presented as movies are available as separate files in the supporting information. Particle tracking was performed using MATLAB routines developed in the laboratory of Prof. Maria Kilfoil [1], and based on the particle tracking algorithm developed by Crocker and Grier[2] Using these multiparticle tracking methods, for mfp-3S-pep coacervate 25,922 of positions were assigned to 264 particle trajectories (collected from 3 movies from 3 fields of view); for mfp-3F-pep / HA coacervate 3,829 of positions were assigned to 41 particle trajectories (collected from 5 movies from 5 fields of view) From these, we calculated the ensemble-averaged mean-squared tracer displacement

$$\langle \Delta x^2(\tau) \rangle = \langle |x(t+\tau) - x(t)|^2 \rangle$$

as a function of lag time τ where the angular brackets indicate an average over many starting times *t* and the ensemble of particles. For a viscous fluid, the particle motion was purely diffusive, and

$$\langle \Delta x^2(\tau) \rangle = 2dD\tau$$

where *d* is the space dimension (here *d*=2), and *D* is the diffusion coefficient. *D* is related to the shear viscosity η through the Stokes-Einstein relation:

$$D = \frac{k_B T}{6\pi\eta a}$$

where k_B is the Boltzmann constant, *T* is temperature, and *a* is the particle radius.

The resulting mean square displacement (MSD) versus time plots are presented in Figure S2. In the case of particles moving within the mfp3f / HA coacervate, we found that the MSD increased linearly with lag time, suggesting purely viscous behavior of the coacervate phase. By linear least-squares fitting we determined the slope of the calculated MSD versus lag time, and using the Stokes-Einstein relation, determined the shear viscosity to be η = 19.4 ± 0.3 Pa·s for mfp-3F-pep / HA coacervate. By contrast, the MSD versus lag time plot obtained for particles trapped in the mfp-3S-pep coacervate phase is not resolvable, although at much longer lag times, we observe superdiffusive motion consistent with convective drift of the microscope stage (not shown). Consequently only lower limit estimate could be given for the viscosity of the mfp-3S-pep coacervate phase η > 1200Pa·s.

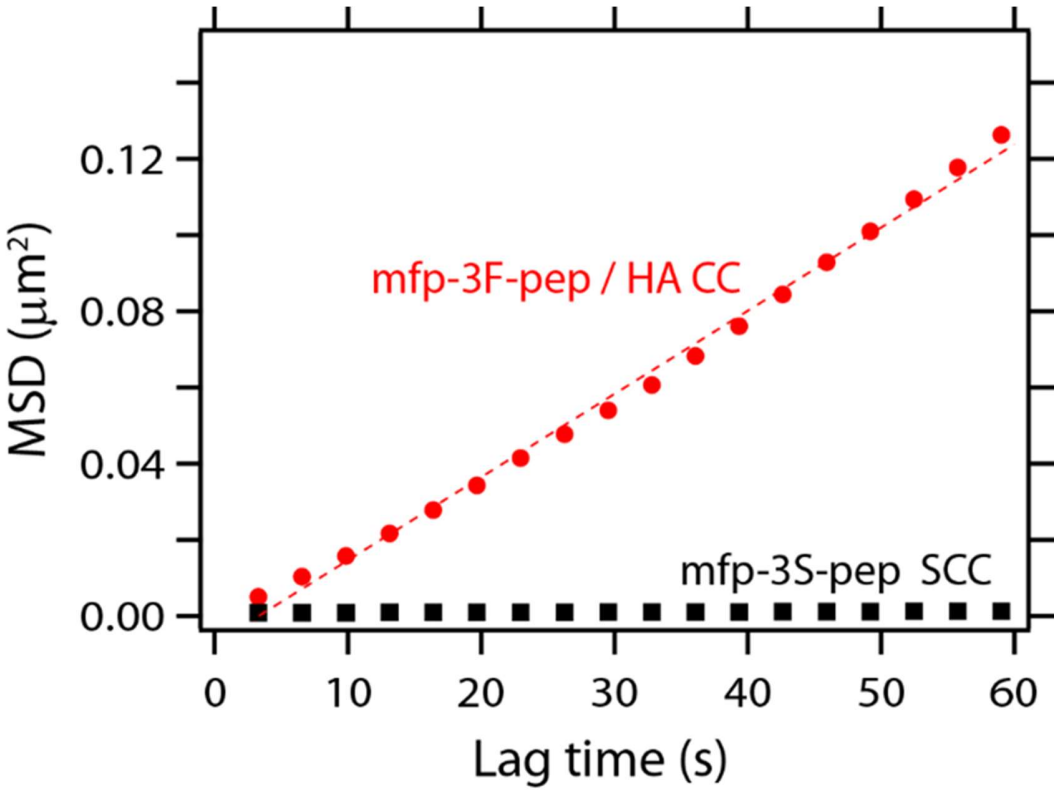

Figure S2. MSD vs time (τ) plot obtained for tracking of 40-nm diameter fluorescent beads in coacervates formed from mfp-3F-pep / HA (red circles) and mfp-3S-pep (black squares) The linear least-squares fit to the mfp-3F-pep / HA data (red dashes) is shown. From this, a viscosity of 19.4±0.3 Pa·s is determined. The motion of the particles in the mfp-3S-pep SCC is not resolvable.

Cryo-TEM

Cryo-TEM specimens were prepared in a controlled environment vitrification system (CEVS) at 25 °C and 100% relative humidity, to prevent evaporation from the specimen, as described elsewhere[3,4]. Before specimen preparation the grids were plasma-etched in a PELCO EasiGlow glow-discharger (Ted Pella Inc., Redding, CA) to improve their hydrophilicity. Because the coacervated liquids are too viscous for thin cryo-TEM specimen preparation, the coacervates were prepared on the grid itself by mixing two equal volumes drops, e.g., of mfp-3F-pep and of hyaluronic acid, about 2 microliters each, on the grid, following by blotting of the mixed liquid to the desirable thickness (up to 300 nm in areas useful for TEM imaging). Imaging was performed with an FEI Tecnai T12 G^2, LaB_6 electron gun-equipped transmission electron microscope, operated at 120 kV. The vitrified specimens were equilibrated in the microscope below -178 °C in a Gatan 626 cryo-holder. We imaged the specimens in the low-dose imaging mode to minimize electron-beam radiation-damage[5]. Images were recorded digitally by a Gatan US1000 CCD camera, using the DigitalMicrograph software package.

EPR measurements

X-band CW EPR spectra were acquired using one of two commercial Bruker EMX EPR spectrometers, one installed in the user facility in the Materials Research Laboratory and the second one in the laboratory of Prof. Songi Han, both at UCSB. Where specified, temperature was controlled using N_2 gas flow using

standard variable temperature accessory. The temperature was stabilized to within 0.1 K for > 1 min prior to the beginning of the measurement. The modulation frequency was 100kHz, modulation amplitude 1G, conversion time 40ms/point, and time constant 20ms. Samples for EPR measurements were prepared in either 0.6mm ID / 0.84OD capillaries (5µl sample volume) or in rectangular 0.4mm by 4mm capillaries (~50 µl sample volume), both purchased from Vitrocom Inc.

EPR spectra were recorded in a dilute solution prior to (Figure S3) and after (Figure S4) the coacervate formation, with mfp-3S-pepSL or mfp-3F-pepSL peptides. In order to rule out that the reduction in spectral resolution and broadening of the lineshape is not mainly due to an increase in spin-spin interactions stemming from an increase in local spin concentrations in the condensed coacervate phase, only 20% of the total peptides were spin-labeled to probe the mfp-3F-pep / HA complex coacervate and 10% of the total peptides spin-labeled to probe the mfp-3S-pepSL simple coacervate system. This scheme of "spin dilution" ensures that the spin labeled peptide serves as reporters of local peptide dynamics and its local environment.

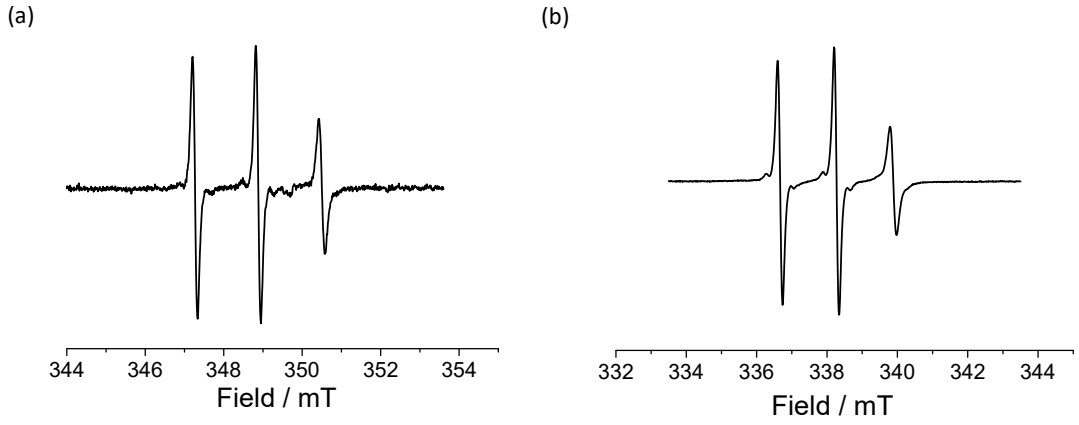

Figure S3. CW EPR spectra of (a) mfp-3F-pepSL and (b) mfp-3S-pep before coacervate formation.

The "before" EPR spectra, acquired in a dilute peptide solution prior to coacervate formation (Figure S3), showed no significant difference in peptide dynamics between the two different mfp-3S peptides, and is constituted of a single spectral component corresponding to a fast tumbling of nitroxide spin labels characteristic of spin labels tethered to soluble unstructured peptides ($\tau_{rot} \approx 100$ps)[6]. The EPR spectra of these peptides upon coacervate formation, however, are distinctly altered (Figure S4). In either system constituting the mfp-3S-pepSL or mfp-3F-pepSL / HA coacervate phase, upon coacervate formation the EPR spectrum clearly resolves two spectral components. The majority (95% in case of mfp-3S-pepSL and 85% in case of mfp-3F-pepSL / HA) component corresponds to a "slow" spectral component of the peptide-tethered spin label showing significantly retarded rotational mobility of the spin label upon coacervate formation. The minority "fast" component is highly similar to the EPR spectra obtained for the peptides prior to the coacervate formation, and thus was assigned to the peptides remaining in the dilute phase. The slowdown of the peptide dynamics is an order of magnitude greater in the mfp-3S-pepSL coacervate with retardation factor of 200 (τ_{rot}~20 ns) than in the mfp-3F-pepSL / HA coacervate phase with retardation factor of 10 (τ_{rot}~1 ns). In contrast, no slowdown in the rotational dynamics of

spin labeled HA was observed upon mfp-3F-pep / HA-SL coacervate formation (Figure S5), suggesting that the compaction of HA and interaction between mfp-3F-pepSL and HA is very weak. This observation is consistent with previous reports of comparable complex coacervate systems consisting of mfp151 and spin-labeled HA[7]. The peptide dynamics is significantly more confined at the molecular level within the mfp-3S-pep compared to the mfp-3F-pepSL / HA coacervate phase. The greater retardation of peptide dynamics implies greater inter-peptide molecular interaction and cohesion.

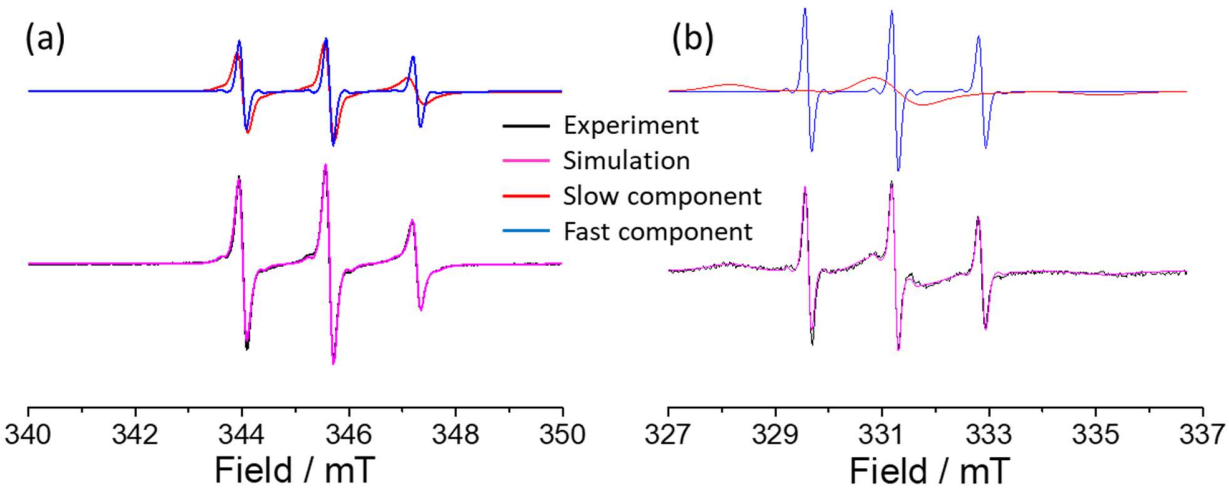

Figure S4. Experimental spectra (black) and two-component simulation (magenta) of CW EPR spectra for mfp-3F-pep (a) and mfp-3S-pep (b); "fast" components are shown in blue and "slow" components are shown in red for both coacervate systems.

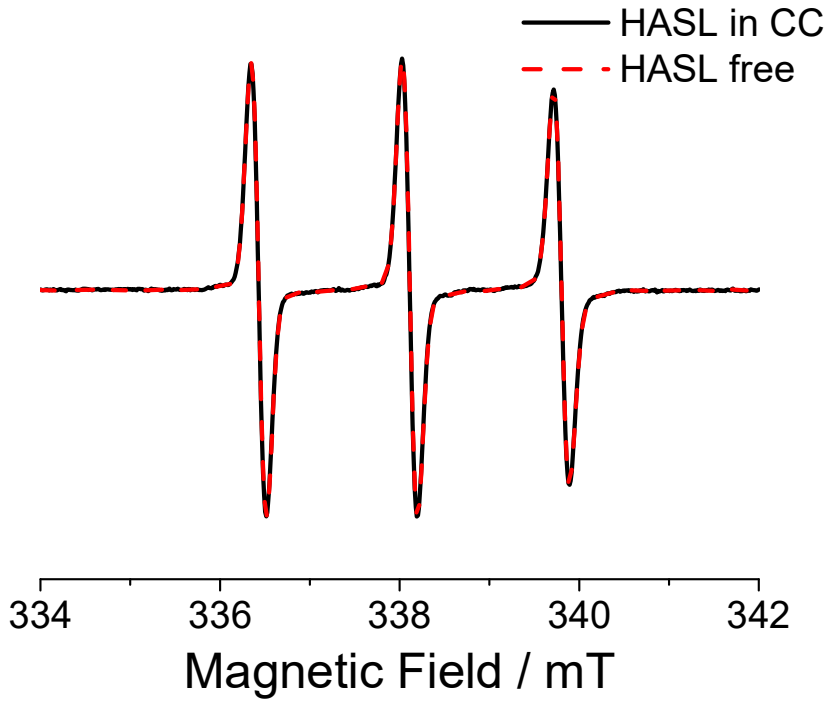

Figure S5. Overlay of CW EPR spectra of spin-labelled HA (HA-SL) free in solution (red) and in mfp-3F-pep HA-SL complex coacervate (black).

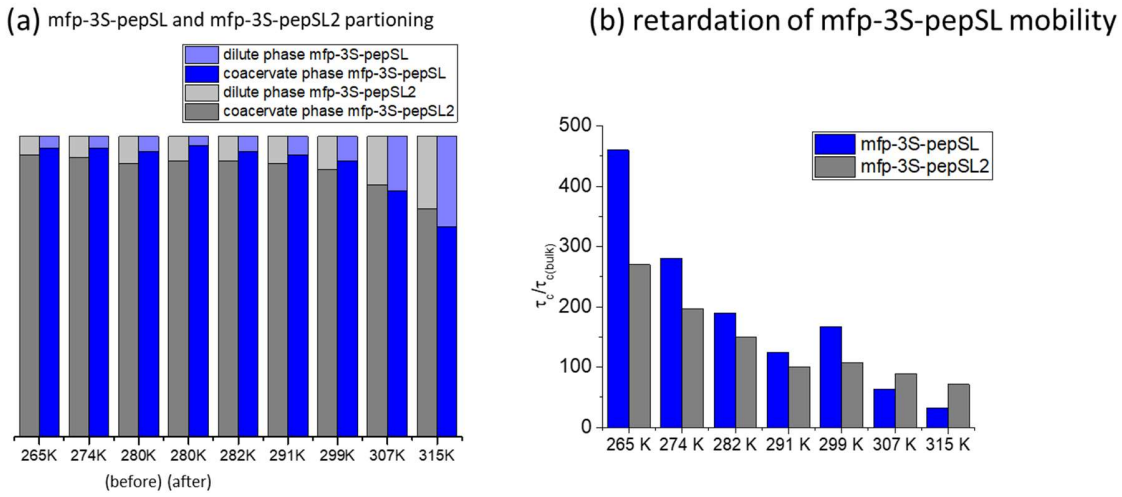

Figure S6. EPR spectroscopy derived (a) individual peptide partitioning between the coacervate and dilute phases as function of temperature for mfp-3S-pepSL and mfp-3S-pepSL2 peptides and (b) individual changes in peptide mobility of mfp-3S-pepSL and mfp-3S-pepSL2 peptides presented as retardation factor in the coacervate phase as function of temperature. (Higher values correspond to slower peptide mobility).

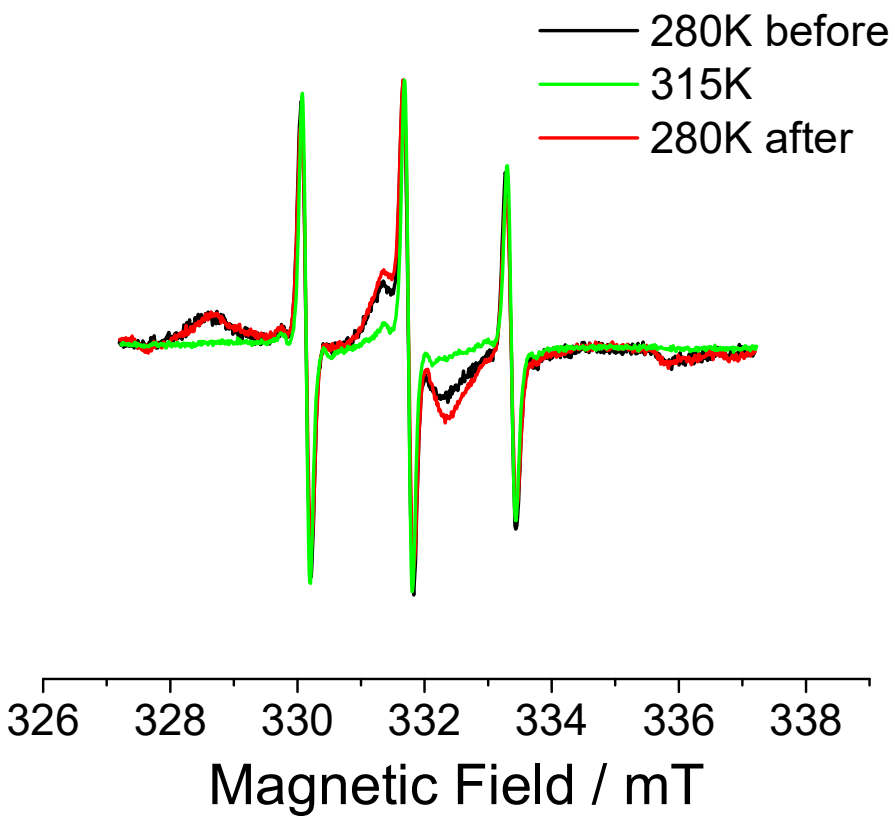

Figure S7. Overlay of the experimental EPR spectra taken on mfp-3S-pepSL coacervate at different points of a temperature dependent series. Black spectrum taken before, green at the maximum temperature and red after the series. .

EPR spectra simulations

CW EPR spectra were simulated using the slow-motion model as implemented in a "MultiComponent" software developed by Dr. Christian Altenbach in the laboratory of Prof. Wayne Hubbell[8], which is based on an earlier implementation of the microscopic order macroscopic disorder (MOMD) algorithm by Budil et. al[9]. Parameters used in simulations were typical for MTSL spin labels: g_{xx} = 2.008; g_{yy} = 2.0055; g_{zz} = 2.002; A_{xx} = 17.4 MHz; A_{yy} = 16.5 MHz; A_{zz} = 103.2 MHz and the same for both spectral components for each of the two peptides. The only parameters that were allowed to vary were (i) individual isotropic rotational correlation for each "fast" and "slow" component and (ii) the ratio between the two components.

ODNP experiment and data processing

ODNP measurements and analysis were performed according to procedure detailed in Franck et. al.[10] which includes sample heating correction. Briefly, In an ODNP experiment an enhancement of the ^{1}H NMR signal *E* is measured as function of applied microwave power *p* on-resonance with the central EPR transition of the nitroxide radical to obtain the $E(p)$. In addition spin-lattice relaxation (T_1) is measured at a subset of the microwave powers used for the enhancement curve to arrive at $T_1(p)$. From these two datasets the concentration-normalized cross-relaxation rate k_σ is calculated:

$$k_\sigma = \lim_{p\to\infty}\left(\frac{1-E(p)}{T_1(p)}\left|\frac{\gamma_H}{\gamma_e}\right|\right)\frac{1}{s_{\max}C}$$

Where $s_{\max}$ is the maximum extent of saturation possible for the nitroxide EPR spectrum and is assumed to be $s_{\max}\approx 1$; *C* is radical concentration; γ_e and γ_H are electron and proton gyromagnetic ratios respectively. The cross relaxation parameter k_σ is directly related to the water mobility in the vicinity of the nitroxide radical through the spectral density function as detailed elsewhere[11,12]. Note that in the regime relevant for this work higher k_σ values correspond to faster water motion around the nitroxide spin-label.

A more common way to analyze ODNP data is by using a coupling factor parameter $\xi = \frac{k_\sigma}{k_\rho}$ where $Ck_\rho = \frac{1}{T_1} - \frac{1}{T_{1,0}}$, however, this approach was not applicable in this work since for most of the measurements T_1 and $T_{1,0}$ were the same within error, thereby precluding determination of k_ρ and consequently the ξ values. (data not shown).

Table S2. Summary of the raw ODNP parameters

	[mfp-3F-pep] = 0.8mg/ml [mfp-3F-pepSL] = 0.2mg/ml		[mfp-3S-pepSL] = 2mg/ml	
	free	coacervate	free	coacervate
maximum enhancement	-3	-2	-17	0.5
T_1 (s)	1.8 ± 0.04s	1.85 ± 0.05s	1.85± 0.05s	1.77± 0.05s
k_σ ($s^{-1}M^{-1}$)	44	26.5	21	6

ODNP measurements were carried out using a home-built add-on module to a commercial Bruker EMX EPR spectrometers described in the EPR measurements section of the SI. The measurements were performed at magnetic field of ~0.35 T corresponding to a proton Larmor frequency of ~14.8 MHz and electron Larmor frequency of ~9.8 GHz. A 3.5 µl sample was loaded into a 0.6 mm i.d., 0.84 mm o.d. quartz capillary tube (VitroCom). The tubes were sealed at one end with beeswax and at the other with critoseal

polymer. A home-built NMR probe that fits into the EPR resonator and was designed to minimally affect the resonator mode was used. The NMR signal was recorded using the heteronuclear X-channel of a commercial 300MHz Bruker AVANCE spectrometer. To minimize microwave-induced heating the sample was cooled down by continuous flow of room temperature nitrogen gas.

Local water density by ESEEM measurements.

To quantify the amount of hydration water expelled from the mfp-3S-pep vicinity upon coacervate formation, we measured the ESEEM spectra of the mfp-3S-pepSL and mfp-3S-pepSL2 before (Figure S8a red trace) and after (Figure S8a black trace) coacervate formation. Samples were prepared with D_2O and significant signal reduction in the intensity of the narrow peak at the ^2H frequency (I_{2H}) in the FT-ESEEM spectra was observed upon formation of the coacervate. (Figure S8a). The narrow ^2H peak was previously shown to originate from water molecules in the second and further hydration shells of the nitroxide radical[13]. Consequently I_{2H} increases monotonically with increase in the density of the surrounding heavy-water molecules and provides a measure of the local D_2O density. To arrive at a quantitative measure for the reduction of the local water density, a series of calibration ESEEM measurements was performed on the mfp-3S-pepSL samples (prior to coacervate formation) with varying D_2O to H_2O ratios. Since in these samples, the density of the ^2H atoms scales linearly with the D_2O / H_2O ratio, it allowed us to make a calibration curve that relates the I_{2H} to the local ^2H density in the vicinity of the mfp-3S-pep peptide. The resulting I_{2H} calibration curve is presented in Figure S8b as black squares. The I_{2H} values corresponding to the mfp-3S-pepSL and mfp-3S-pepSL2 in the coacervate phase are shown as filled and empty red circles respectively in Figure S8b. The points in the calibration curve were fitted with a 2nd order polynomial (red curve in Figure S8b) and the local D_2O concentration for the mfp-3S-pepSL and mfp-3S-pepSL2 peptide in the coacervate phase was calculated from this fit. It was found to be 35% and 45% respectively where the data were normalized such that the 100% value was taken as the I_{2H} value obtained for mfp-3S-pepSL in 100% D_2O prior to coacervate formation. The I_{2H} for the mfp-3S-pepSL2 in 100% D_2O was the same as for mfp-3S-pepSL under identical conditions.

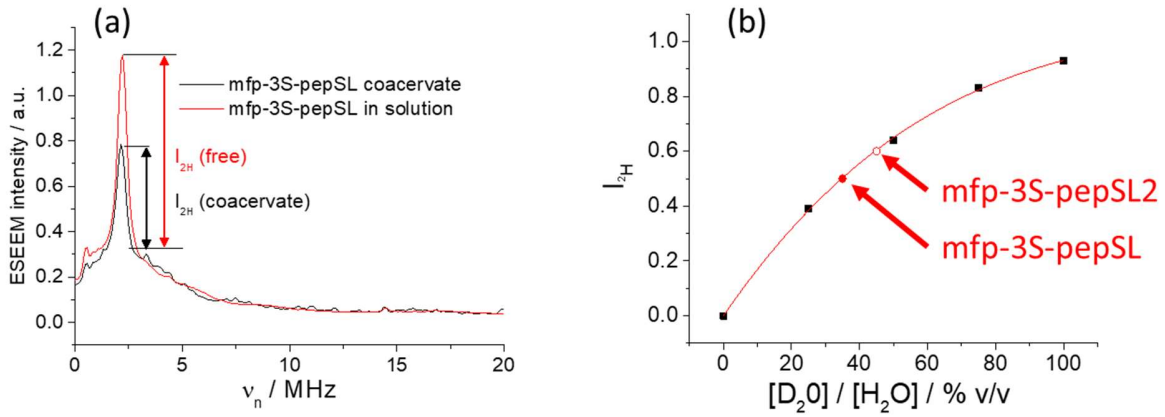

Figure S 8. (a) FT-ESEEM spectra for mfp3-3S-pepSL free in solution (red) and in the coacervate phase (black). (b) Black points: I_{2H} as function of $[D_2O]$ / $[H_2O]$ for free mfp-3S-pepSL in dilute solution. Red points: I_{2H} for mfp-3S-pepSL (closed circle) and mfp-3S-pepSL2 (open circle) in the coacervate phase. FT- ESEEM spectra taken on mfp-3S-pepSL samples prepared with D_2O and 30% sucrose added as cryoprotectant.

ESEEM sample preparation: To allow for freezing of the coacervate sample without formation of crystalline ice the coacervate samples were supplemented with sucrose to a final concentration of 30% w/v. The sucrose powder was completely dissolved using a peptide stock solution before NaCl was added to form a coacervate phase. For ESEEM measurements peptide stock solutions (for mfp-3S-pep and mfp-3S-pepSL) and NaCl stock solutions were prepared with D_2O instead of H_2O. The formation of the coacervate phase was confirmed by observing the increase in the turbidity of the solution upon addition of NaCl. For the samples used to create the ESEEM calibration curve, where no coacervate was formed the NaCl solution was substituted by the equivalent amount of water or D_2O.

For ESEEM measurements 50µl of the sample solution were transferred into a 3mm O.D. quartz EPR tube (Vitrocom), flash frozen in liquid nitrogen and inserted into a precooled cryostat. ESEEM measurements were performed using commercial Bruker Elexsys E380 Spectrometer equipped with MS3 flexline resonator; a liquid nitrogen flow cryostat (Oxford Instruments) was used to maintain the temperature. The pulse sequence was π/2-τ-π/2-T-π/2-τ-echo. The echo intensity was recorded as function of interpulse delay T. Experimental parameters were: π/2 = 16ns; τ = 204ns; T was incremented from 96ns with 24ns increments; temperature was set to 85K. Data processing: the background decay was subtracted using a bi-exponential fit, the resulting trace was zero filled to 4096 points, apodized by a hamming function and Fourier transformed to obtain FT-ESEEM spectrum.

Hydropathy

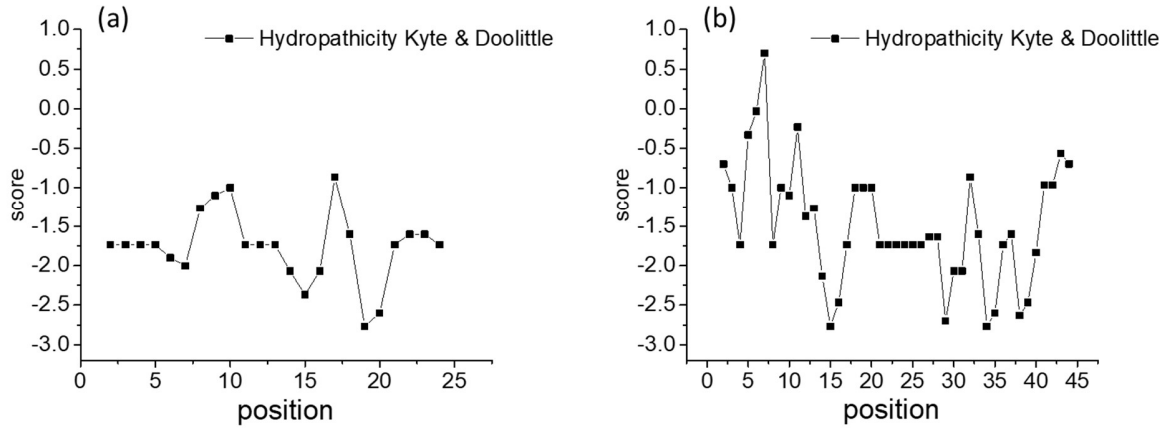

Figure S 9. Hydropathy on Kyte and Doolittle scale[14] for mfp-3S-pep (a) and full length mfp-3S protein (b) as calculated using the ProtScale ExPASy server. Window size was set to 3 and relative weight of the window edges compared to the window center was 100 percent.

SFA

Briefly, in SFA experiments the absolute distance between back-silvered mica surfaces in a cross-cylinder geometry is measured, typically with interferometry, and the force, *F*, is measured by the deflection of a cantilever spring. All forces are normalized by the radius of curvature, *R*, of the cylindrical silica disks to which the mica surfaces are glued. Values for the adhesive force, F_{ad}/R, are given by the depth of forces into the attractive regime before the jump out, a mechanical instability dependent on spring stiffness[15].

Before each SFA experiment, the two mica surfaces were brought into contact in air to calibrate the absolute zero of separation distance. Next, 80 ul of the freshly-mixed coacervate solution was deposited

onto one of the surfaces and was allowed to settle for 60 minutes. The turbidity of the coacervate mixtures prevented accurate interferometric measurements of surface separation after the jump out, and consequently a strain gauge was used for all measurements of adhesive force. However, optical interferometry was possible at short distances (D < 5 μm), allowing for visualization of the profile of the surfaces while in contact using the fringes of equal chromatic order (FECO). During each force run, the base of the cantilever spring was moved with a motorized micrometer either toward or away from the opposing surface at a constant speed, which ranged from 10 to 240 nm/s.

References

(1) Pelletier, V.; Gal, N.; Fournier, P.; Kilfoil, M. L. *Phys. Rev. Lett.* **2009**, *102* (18).
(2) Crocker, J. C.; Grier, D. G. *J. Colloid Interface Sci.* **1996**, *179* (1), 298.
(3) Bellare, J. R.; Davis, H. T.; Scriven, L. E.; Talmon, Y. *J. Electron Microsc. Tech.* **1988**, *10* (1), 87.
(4) Talmon, Y. *J. Mol. Liq.* **2015**, *210*, 2.
(5) Yan, Y.; Hoffmann, H.; Makarsky, A.; Richter, W.; Talmon, Y. *J. Phys. Chem. B* **2007**, *111* (23), 6374.
(6) Drescher, M. In *EPR Spectroscopy*; Topics in Current Chemistry; Springer, Berlin, Heidelberg, 2011; pp 91–119.
(7) Ortony, J. H.; Hwang, D. S.; Franck, J. M.; Waite, J. H.; Han, S. *Biomacromolecules* **2013**, *14* (5), 1395.
(8) Altenbach, C.; López, C. J.; Hideg, K.; Hubbell, W. L. *Methods Enzymol.* **2015**, *564*, 59.
(9) Budil, D. E.; Lee, S.; Saxena, S.; Freed, J. H. *J. Magn. Reson. A* **1996**, *120*, 155.
(10) Franck, J. M.; Pavlova, A.; Scott, J. A.; Han, S. *Prog. Nucl. Magn. Reson. Spectrosc.* **2013**, *74*, 33.
(11) Hausser, K. H.; Stehlik, D. *Adv Magn Reson* **1968**, *3*, 79.
(12) Hwang, L.-P.; Freed, J. H. *J. Chem. Phys.* **1975**, *63* (9), 4017.
(13) Erilov, D. A.; Bartucci, R.; Guzzi, R.; Shubin, A. A.; Maryasov, A. G.; Marsh, D.; Dzuba, S. A.; Sportelli, L. *J. Phys. Chem. B* **2005**, *109* (24), 12003.
(14) Kyte, J.; Doolittle, R. F. *J. Mol. Biol.* **1982**, *157* (1), 105.
(15) Israelachvili, J.; Min, Y.; Akbulut, M.; Alig, A.; Carver, G.; Greene, W.; Kristiansen, K.; Meyer, E.; Pesika, N.; K Rosenberg; Zeng, H. *Rep. Prog. Phys.* **2010**, *73* (3), 036601.